

# Analysis of Bose-Einstein correlations at fixed multiplicities in TeV energy $pp$ collisions in the quantum optical approach

N.Suzuki\*

*Department of comprehensive management,  
Matsumoto University, Matsumoto 390-1295, Japan*

M. Biyajima†

*Department of physics, Shinshu University, Matsumoto 390-8621, Japan*

(Dated: March 26, 2013)

## Abstract

The multiplicity distribution and the two-particle Bose-Einstein correlations at fixed multiplicities observed in  $pp$  collisions at  $\sqrt{s} = 7$  TeV by the ALICE Collaboration are analyzed by the formulae obtained in the quantum optical approach. The chaoticity parameters in the inclusive and semi-inclusive events are estimated from the analysis. Multiplicity or  $k_T$  dependence of longitudinal and transverse source radii are also estimated.

PACS numbers: 25.75.Gz

---

\* suzuki@matsu.ac.jp

† biyajma@azusa.shinshu-u.ac.jp

## I. INTRODUCTION

In high energy nucleus-nucleus or hadron-hadron collisions, Bose-Einstein correlations of identical particles are considered as one of the possible measures for the space-time domain where those particles are produced. As the colliding energy increases up to the TeV region, Bose-Einstein correlations of identical particles can be precisely analyzed in the semi-inclusive events or at fixed multiplicities to estimate the production domain of identical particles.

Up to the present, most of theoretical approaches to identical particle correlations in the semi-inclusive events are investigated in the case of purely chaotic field [1–4].

One of the theoretical approaches to the Bose-Einstein correlations is made on the analogy of the quantum optics [5, 6], where two types of sources, chaotic and coherent sources are introduced. A diagrammatical method, based on the Glauber-Lachs formula [5] which is derived from the single-mode laser optics, has been proposed [7] to find higher order Bose-Einstein correlation (BEC) functions in the inclusive events. In Ref.[8], the generating functional (GF) for the momentum densities is formulated, and a diagrammatic representation for the cumulants is proposed. Identical particle correlations in the semi-inclusive events are formulated in [9]. It is shown [10] that the multiplicity distribution (MD) in the quantum optical (QO) approach is approximately given by the Glauber-Lachs formula [5, 11].

In general, in the formulation of two-particle BEC function at fixed multiplicities or in the semi-inclusive events, two-particle and one-particle momentum densities in the semi-inclusive events and the MD are contained. If the two-particle momentum density is integrated over one of the momenta, the one-particle momentum density is obtained. If the one-particle density is integrated over, the MD is obtained [12]. Therefore, even in the observed MD, information on the source radii would be included.

In the present paper, the MD and the two-particle Bose-Einstein correlations in the semi-inclusive events observed by the ALICE Collaboration are analyzed by the formulae obtained in the QO approach. The chaoticity parameter  $p_{\text{in}}$  in the inclusive events is estimated from the analysis of the observed charged MD. The chaoticity parameter  $p_{\text{sm}}$  in the semi-inclusive events is estimated from the analysis of two-particle Bose-Einstein correlations. Longitudinal and transverse source radii at fixed multiplicities are also estimated from the data.

## II. MOMENTUM DENSITIES IN THE SEMI-INCLUSIVE EVENTS

In the QO approach, the  $n$ -particle momentum density in the semi-inclusive events is defined by,

$$\rho_n(p_1, \dots, p_n) = c_0 \langle |f(p_1)|^2 \cdots |f(p_n)|^2 \rangle_a, \quad n = 1, 2, \dots$$

$$f(p) = \sum_{i=1}^M a_i \phi_i(p) + f_c(p), \quad (1)$$

where  $c_0$  is a normalization factor. In Eq.(1),  $\phi_i(p)$  and  $f_c(p)$  are amplitudes of the  $i$ th chaotic source and a coherent source, respectively, and  $a_i$  is a random complex number attached to the  $i$ th chaotic source. In addition,  $M$  is the number of independent chaotic sources[8], which is regarded to be infinite in the present paper.

In Eq.(1), parenthesis  $\langle F \rangle_a$  denotes an average of  $F$  over the random number  $a_i$  with a Gaussian weight [6];

$$\langle F \rangle_a = \prod_{i=1}^M \left( \frac{1}{\pi \lambda_i} \int \int \exp\left[-\frac{|a_i|^2}{\lambda_i}\right] d^2 a_i \right) F. \quad (2)$$

One-particle and two-particle momentum densities are respectively given as,

$$\rho_1(p_1) = c_0 \langle |f(p_1)|^2 \rangle_a = c_0 [r(p_1, p_1) + c(p_1, p_1)], \quad (3)$$

$$\begin{aligned} \rho_2(p_1, p_2) &= c_0 \langle |f(p_1) f(p_2)|^2 \rangle_a \\ &= c_0 \{ \rho(p_1) \rho(p_2) + |r(p_1, p_2)|^2 + 2 \text{Re}[r(p_1, p_2) c(p_2, p_1)] \}, \end{aligned} \quad (4)$$

where  $r(p_1, p_2)$  is a correlation caused by the chaotic sources and  $c(p_1, p_2)$  is a correlation by the coherent source,

$$r(p_1, p_2) = \sum_{i=1}^M \lambda_i \phi_i(p_1) \phi_i^*(p_2), \quad c(p_1, p_2) = f_c(p_1) f_c^*(p_2). \quad (5)$$

The generating functional (GF) of momentum densities in the semi-inclusive events is defined by the following equation [12],

$$Z_{\text{sm}}[h(p)] = \sum_{n=1}^{\infty} \frac{1}{n!} \int \cdots \int \rho_n(p_1, \dots, p_n) h(p_1) \cdots h(p_n) \frac{d^3 p_1}{E_1} \cdots \frac{d^3 p_n}{E_n}. \quad (6)$$

From Eqs.(1), (2) and (6), the GF is written as,

$$Z_{\text{sm}}[h(p)] = c_0 \left\langle \exp \left[ \int \int \int |f(p)|^2 h(p) \frac{d^3 p}{E} \right] \right\rangle_a, \quad (7)$$

where an additional constant  $Z_{\text{sm}}[h(p) = 0](= c_0)$  is added to the right hand side of Eq.(6).

Inversely, the  $n$ -particle momentum density in the semi-inclusive events is given from the GF as

$$\rho_n(p_1, \dots, p_n) = E_1 \cdots E_n \frac{\delta^n Z_{\text{sm}}[h(p)]}{\delta h(p_1) \cdots \delta h(p_n)} \Big|_{h(p)=0}. \quad (8)$$

The  $n$ th order cumulant is given by

$$g_n(p_1, \dots, p_n) = E_1 \cdots E_n \frac{\delta^n \ln Z_{\text{sm}}[h(p)]}{\delta h(p_1) \cdots \delta h(p_n)} \Big|_{h(p)=0}. \quad (9)$$

From Eqs.(8) and (9), we have an iteration relation for the momentum densities [9],

$$\begin{aligned} \rho_1(p_1) &= c_0 g_1(p_1), \\ \rho_n(p_1, \dots, p_n) &= g_1(p_1) \rho_{n-1}(p_2, \dots, p_n) + c_0 g_n(p_1, \dots, p_n) \\ &\quad + \sum_{i=1}^{n-2} \sum g_{i+1}(p_1, p_{j_1}, \dots, p_{j_i}) \rho_{n-i-1}(p_{j_{i+1}}, \dots, p_{j_{n-1}}). \end{aligned} \quad (10)$$

The second summation on the right hand side of Eq.(10) indicates that all possible combinations of  $(j_1, \dots, j_i)$  and  $(j_{i+1}, \dots, j_{n-1})$  are taken from  $(2, 3, \dots, n)$ .

In order to calculate momentum densities at fixed multiplicities, following equations are defined for  $n = 1, 2, \dots$  and  $k = 0, 1, \dots, n-1$ ;

$$\begin{aligned} \rho_n^{(k)}(p_1, \dots, p_k) &= \frac{1}{(n-k)!} \int \cdots \int \rho_n(p_1, \dots, p_k, p_{k+1}, \dots, p_n) \frac{d^3 p_{k+1}}{E_{k+1}} \cdots \frac{d^3 p_n}{E_n}, \\ g_n^{(k)}(p_1, \dots, p_k) &= \frac{1}{(n-k)!} \int \cdots \int g_n(p_1, \dots, p_k, p_{k+1}, \dots, p_n) \frac{d^3 p_{k+1}}{E_{k+1}} \cdots \frac{d^3 p_n}{E_n}. \end{aligned} \quad (11)$$

Then the MD is given by

$$\begin{aligned} P(0) &= c_0, \\ P(n) &= \rho_n^{(0)} = \frac{(n-k)!}{n!} \int \cdots \int \rho_n^{(k)}(p_1, \dots, p_k) \frac{d^3 p_1}{E_1} \cdots \frac{d^3 p_k}{E_k}. \end{aligned} \quad (12)$$

From Eqs.(10), (11) and (12), we have

$$P(n) = \frac{1}{n} \sum_{j=1}^n j g_j^{(0)} P(n-j) = \frac{1}{n} \sum_{j=1}^n [\Delta_j^{(R)} + j \Delta_{j-1}^{(S)}] P(n-j), \quad (13)$$

$$\rho_n^{(1)}(p_1) = \sum_{j=1}^n j g_j^{(1)}(p_1) P(n-j), \quad g_j^{(1)}(p_1) = R_j(p_1, p_1) + \sum_{l=0}^{j-1} T_{l,j-l-1}(p_1, p_1), \quad (14)$$

$$\begin{aligned}
\rho_n^{(2)}(p_1, p_2) &= \sum_{j=1}^{n-1} (n-j) g_j^{(1)}(p_1) \rho_{n-j}^{(1)}(p_2) + \sum_{j=2}^n g_j^{(2)}(p_1, p_2) P(n-j), \\
g_j^{(2)}(p_1, p_2) &= \sum_{l=1}^{j-1} R_j(p_1, p_2) R_{j-l}(p_2, p_1) \\
&+ \sum_{l=0}^{j-2} \sum_{m=0}^l \{ T_{m, l-m}(p_1, p_2) R_{j-l-1}(p_2, p_1) + R_{j-l-1}(p_1, p_2) T_{m, l-m}(p_2, p_1) \}, \quad (15)
\end{aligned}$$

where, with  $R_0(k_1, k_2) = \omega_1 \delta^3(\mathbf{k}_1 - \mathbf{k}_2)$ ,

$$\Delta_j^{(R)} = \int \int \int R_j(k, k) \frac{d^3 k}{\omega}, \quad \Delta_{j-1}^{(S)} = \int \int \int T_{0, j-1}(k, k) \frac{d^3 k}{\omega}, \quad (16)$$

$$\begin{aligned}
R_j(p_1, p_2) &= \int \int \int r(p_1, k) R_{j-1}(k, p_2) \frac{d^3 k}{\omega}, \\
T_{j, l}(p_1, p_2) &= \int \cdots \int R_j(p_1, k_1) c(k_1, k_2) R_l(k_2, p_2) \frac{d^3 k_1}{\omega_1} \frac{d^3 k_2}{\omega_2}. \quad (17)
\end{aligned}$$

If Eq.(15) for  $\rho_n^{(2)}(p_1, p_2)$  is integrated over  $p_2$ , Eq.(14) for  $\rho_n^{(1)}(p_1)$  is obtained. In addition, if Eq.(14) is integrated, Eq.(13), the recurrence equation for the MD, is obtained.

### III. PARAMETRIZATION

In the followings, variables are changed from  $(p_{1L}, \mathbf{p}_{1T})$  to  $(y_1, \mathbf{p}_{1T})$  with rapidity  $y_1$  defined by  $y_1 = \tanh^{-1}(p_{1L}/E_1)$ . Correlations  $r(p_1, p_2)$  and  $c(p_1, p_2)$  are both assumed to be real, and are parametrized as [9],

$$\begin{aligned}
r(y_1, \mathbf{p}_{1T}; y_2, \mathbf{p}_{2T}) &= p_{\text{sm}} \sqrt{\rho(y_1, \mathbf{p}_{1T}) \rho(y_2, \mathbf{p}_{2T})} I(\Delta y, \Delta \mathbf{p}_{1T}), \\
c(y_1, \mathbf{p}_{1T}; y_2, \mathbf{p}_{2T}) &= (1 - p_{\text{sm}}) \sqrt{\rho(y_1, \mathbf{p}_{1T}) \rho(y_2, \mathbf{p}_{2T})}, \quad (18)
\end{aligned}$$

$$\begin{aligned}
\rho(y_1, \mathbf{p}_{1T}) &= \langle n_0 \rangle \frac{\sqrt{\alpha} \beta}{\pi^{3/2}} \exp[-\alpha y_1^2 - \beta \mathbf{p}_{1T}^2], \\
I(\Delta y, \Delta \mathbf{p}_T) &= \exp[-\gamma_L (\Delta y)^2 - \gamma_T (\Delta \mathbf{p}_T)^2], \quad (19)
\end{aligned}$$

where  $\Delta y = y_2 - y_1$  and  $\Delta \mathbf{p}_T = \mathbf{p}_{2T} - \mathbf{p}_{1T}$ . Six parameters,  $p_{\text{sm}}$ ,  $\langle n_0 \rangle$ ,  $\alpha$ ,  $\beta$ ,  $\gamma_L$  and  $\gamma_T$  are included in Eqs.(18) and (19). All of them are assumed to be positive constant at present: Parameter  $p_{\text{sm}}$  denotes the chaoticity parameter in the semi-inclusive events with  $0 < p_{\text{sm}} < 1$ . Parameter  $\langle n_0 \rangle$  is related to an average multiplicity. In the limit of  $p_{\text{sm}} = 0$ , the MD defined by Eq.(12) or Eq.(13) becomes the Poisson distribution with an average  $\langle n_0 \rangle$ . Parameters  $\alpha$  and  $\beta$  are related to the width of rapidity and  $p_T$  distributions, respectively. The longitudinal momentum transfer squared,  $q_{\text{long}}^2 = (E_1 - E_2)^2 - (p_{1L} - p_{2L})^2$ ,

is approximately written as  $q_{\text{long}}^2 \approx 2\langle m_T^2 \rangle (\cosh \Delta y - 1)$  with the average of transverse mass squared  $\langle m_T^2 \rangle$ . Then,  $q_{\text{long}}^2 \approx \langle m_T^2 \rangle (\Delta y)^2$  for  $|\Delta y| \ll 1$ . Therefore,  $\sqrt{\gamma_L / \langle m_T^2 \rangle}$  is roughly equal to the longitudinal source radius. Similarly,  $\sqrt{\gamma_T}$  denotes the transverse source radius.

Then, the  $j$ th order correlation,  $R_j(p_1, p_2)$ , of chaotic component is written in the following form,

$$R_j(y_1, \mathbf{p}_{1T}, y_2, \mathbf{p}_{2T}) = N_j \exp[-A_j(y_1^2 + y_2^2) + 2C_j y_1 y_2] \\ \times \exp[-U_j(\mathbf{p}_{1T}^2 + \mathbf{p}_{2T}^2) + 2W_j \mathbf{p}_{1T} \mathbf{p}_{2T}], \quad (20)$$

where

$$A_1 = \frac{\alpha}{2} + \gamma_L, \quad A_{j+1} = A_1 - \frac{\gamma_L^2}{A_j + A_1}, \\ C_1 = \gamma_L, \quad C_{j+1} = \frac{\gamma_L C_j}{A_j + A_1}, \\ U_1 = \frac{\beta}{2} + \gamma_T, \quad U_{j+1} = U_1 - \frac{\gamma_T^2}{U_j + U_1}, \\ W_1 = \gamma_T, \quad W_{j+1} = \frac{\gamma_T W_j}{U_j + U_1}, \\ N_1 = p_{\text{sm}} \langle n_0 \rangle \frac{\sqrt{\alpha} \beta}{\pi^{3/2}}, \quad N_{j+1} = \frac{p_{\text{sm}} \langle n_0 \rangle \sqrt{\alpha} \beta}{\sqrt{A_j + A_1} (U_j + U_1)} N_j.$$

Recurrence equations for  $A_j$ ,  $C_j$ ,  $U_j$ ,  $W_j$  and  $N_j$  can be solved [3, 10], and

$$A_j = \frac{r_2 - r_1}{2} \frac{1 + (r_1/r_2)^j}{1 - (r_1/r_2)^j}, \quad C_j = (r_2 - r_1) \frac{(r_1/r_2)^{j/2}}{1 - (r_1/r_2)^j}, \\ U_j = \frac{t_2 - t_1}{2} \frac{1 + (t_1/t_2)^j}{1 - (t_1/t_2)^j}, \quad W_j = (t_2 - t_1) \frac{(t_1/t_2)^{j/2}}{1 - (t_1/t_2)^j}, \\ N_j = \frac{\sqrt{r_2} t_2}{\pi^{3/2}} \left( \frac{p_{\text{sm}} \langle n_0 \rangle \alpha^{1/2} \beta}{r_2^{1/2} t_2} \right)^j \left\{ \frac{1 - (r_1/r_2)}{1 - (r_1/r_2)^j} \right\}^{1/2} \frac{1 - (t_1/t_2)}{1 - (t_1/t_2)^j}, \quad (21)$$

where

$$r_1 = \frac{\alpha + 2\gamma_L - \sqrt{\alpha^2 + 4\alpha\gamma_L}}{2}, \quad r_2 = \frac{\alpha + 2\gamma_L + \sqrt{\alpha^2 + 4\alpha\gamma_L}}{2}, \\ t_1 = \frac{\beta + 2\gamma_T - \sqrt{\beta^2 + 4\beta\gamma_T}}{2}, \quad t_2 = \frac{\beta + 2\gamma_T + \sqrt{\beta^2 + 4\beta\gamma_T}}{2}. \quad (22)$$

#### IV. ANALYTICAL FORMULA FOR MULTIPLICITY DISTRIBUTION

From Eq.(21), the recurrence equation for the MD, Eq.(13), is written as

$$\begin{aligned} P(n) &= \frac{1}{n} \sum_{j=1}^n [\Delta_j^{(R)} + j\Delta_{j-1}^{(S)}] P(n-j), \quad n = 1, 2, \dots, \\ \Delta_j^{(R)} &= \xi^j \{1 - (r_1/r_2)^{j/2}\}^{-1} \{1 - (t_1/t_2)^{j/2}\}^{-2}, \\ \Delta_{j-1}^{(S)} &= A_0 \xi^{j-1} \{1 - (r_1/r_2)^j\}^{-1/2} \{1 - (t_1/t_2)^j\}^{-1}, \end{aligned} \quad (23)$$

where

$$\begin{aligned} \xi &= \frac{p_{\text{sm}} \langle n_0 \rangle \sqrt{\alpha} \beta}{\sqrt{r_2} t_2} = (1 - \sqrt{r_1/r_2}) (1 - \sqrt{t_1/t_2})^2 p_{\text{sm}} \langle n_0 \rangle, \\ A_0 &= \sqrt{1 - r_1/r_2} (1 - t_1/t_2) (1 - p_{\text{sm}}) \langle n_0 \rangle. \end{aligned} \quad (24)$$

As can be seen from the above equations, the MD contains four parameters,  $p_{\text{sm}}$ ,  $\langle n_0 \rangle$ ,  $h_L = \gamma_L/\alpha$  and  $h_T = \gamma_T/\beta$ .

The analytical formula for the MD can be obtained approximately from Eq.(23) [10]. The generating function for  $P(n)$  is defined by

$$\Pi(z) = \sum_{j=0}^{\infty} P(n) z^n.$$

Then, the differential equation for  $\Pi(z)$  is obtained from Eq.(23) as,

$$\frac{d}{dz} \Pi(z) = \sum_{j=1}^{\infty} \left( \Delta_j^{(R)} + j\Delta_{j-1}^{(S)} \right) z^{j-1} \Pi(z). \quad (25)$$

It is shown from Eq.(22) that  $0 < r_1/r_2 < 1$  and  $0 < t_1/t_2 < 1$ . Therefore, for  $r_1/r_2, t_1/t_2 \ll 1$  or  $j \gg 1$ , Eqs.(23) can be approximated by,

$$\Delta_j^{(R)} \simeq \xi^j, \quad \Delta_{j-1}^{(S)} \simeq A_0 \xi^{j-1}.$$

Then, Eq.(25) can be rewritten as,

$$\frac{d\Pi}{\Pi} = \left[ \frac{\xi}{1 - \xi z} + A_0 \xi^{-1} \frac{d}{dz} \left\{ \frac{1}{1 - \xi z} \right\} \right] dz.$$

With the boundary condition  $\Pi(1) = 1$ , we obtain

$$\Pi(z) = \left\{ 1 - \frac{\xi}{1 - \xi} (z - 1) \right\}^{-1} \exp \left[ \frac{A_0}{(1 - \xi)^2} \frac{(z - 1)}{1 - \frac{\xi}{1 - \xi} (z - 1)} \right].$$

The average multiplicity  $\langle n \rangle$  is given from  $\Pi(z)$  as

$$\langle n \rangle = \left. \frac{d\Pi(z)}{dz} \right|_{z=1} = \frac{\xi}{1-\xi} + \frac{A_0}{(1-\xi)^2}. \quad (26)$$

From Eq.(24), parameter  $\xi$  is proportional to  $p_{\text{sm}}\langle n_0 \rangle$ , whereas  $A_0$  is to  $(1-p_{\text{sm}})\langle n_0 \rangle$ . Therefore, from Eqs.(18) and (19), we can identify the first term on the right hand side of Eq.(26) as a contribution of the chaotic sources and the second term that of the coherent source to the average multiplicity  $\langle n \rangle$  ;

$$\frac{\xi}{1-\xi} = p_{\text{in}}\langle n \rangle, \quad \frac{A_0}{(1-\xi)^2} = (1-p_{\text{in}})\langle n \rangle, \quad (27)$$

where  $p_{\text{in}}$  denotes the chaoticity parameter in the inclusive events.

Then, the generation function is given as

$$\Pi(z) = \{1 - p_{\text{in}}\langle n \rangle(z-1)\}^{-1} \exp\left[(1-p_{\text{in}})\langle n \rangle \frac{(z-1)}{1-p_{\text{in}}\langle n \rangle(z-1)}\right]. \quad (28)$$

The MD is given from the GF as

$$\begin{aligned} P(n) &= \frac{1}{n!} \left. \frac{d^n}{dz^n} \Pi(z) \right|_{z=0} \\ &= \frac{(p_{\text{in}}\langle n \rangle)^n}{(1+p_{\text{in}}\langle n \rangle)^{n+1}} \exp\left[-\frac{(1-p_{\text{in}})\langle n \rangle}{1+p_{\text{in}}\langle n \rangle}\right] L_n\left(\frac{(1-p_{\text{in}})\langle n \rangle}{1+p_{\text{in}}\langle n \rangle}\right), \quad n = 0, 1, \dots, \end{aligned} \quad (29)$$

where  $L_n(x)$  denotes the Laguerre polynomial. Equation (29) is called the Glauber-Lachs formula [5, 10, 11]. The KNO scaling function of the Glauber-Lachs formula is given by,

$$\phi(z) = \frac{1}{p_{\text{in}}} \exp\left[-\frac{z+1-p_{\text{in}}}{p_{\text{in}}}\right] I_0\left(\frac{2}{p_{\text{in}}} \sqrt{(1-p_{\text{in}})z}\right), \quad (30)$$

where  $I_0(z)$  is the modified Bessel function.

## V. TWO-PARTICLE BEC FUNCTION

The two-particle Bose-Einstein correlation (BEC) function  $C_n^{(2)}(\Delta y, \Delta \mathbf{p}_T)$  at fixed multiplicity  $n$  is defined as

$$C_n^{(2)}(\Delta y, \Delta \mathbf{p}_T) = \frac{nP(n)}{n-1} \frac{\int \int \int \rho_n^{(2)}(y_1, \mathbf{p}_{1T}, y_1 + \Delta y, \mathbf{p}_{1T} + \Delta \mathbf{p}_T) dy_1 d^2 \mathbf{p}_{1T}}{\int \int \int \rho_n^{(1)}(y_1, \mathbf{p}_{1T}) \rho_n^{(1)}(y_1 + \Delta y, \mathbf{p}_{1T} + \Delta \mathbf{p}_T) dy_1 d^2 \mathbf{p}_{1T}}. \quad (31)$$

Each term in  $\rho_n^{(2)}(p_1, p_2)$  or  $\rho_n^{(1)}(p_1)\rho_n^{(1)}(p_2)$  in Eq.(31) takes the following form,

$$\begin{aligned} F(y_1, \mathbf{p}_{1T}, y_2, \mathbf{p}_{2T}) &= C_0 \exp[-A_{11}y_1^2 - A_{22}y_2^2 + 2A_{12}y_1y_2] \\ &\quad \times \exp[-U_{11}\mathbf{p}_{1T}^2 - U_{22}\mathbf{p}_{2T}^2 + 2U_{12}\mathbf{p}_{1T}\mathbf{p}_{2T}], \end{aligned} \quad (32)$$



where  $y_2 = y_1 + \Delta y$ ,  $\mathbf{p}_{2T} = \mathbf{p}_{1T} + \Delta \mathbf{p}_T$ .  $C_0$ ,  $A_{11}$ ,  $A_{12}$ ,  $A_{22}$ ,  $U_{11}$ ,  $U_{12}$  and  $U_{22}$  are some constants.

In the observed Bose-Einstein correlations by the ALICE Collaboration [13], the average  $\mathbf{k}_T$  of the two particle transverse momenta is restricted in a small region. In order to take the constraint into account, we parametrize,  $\mathbf{p}_{1T} = \mathbf{k}_T - \Delta \mathbf{p}_T/2$ , and  $\mathbf{p}_{2T} = \mathbf{k}_T + \Delta \mathbf{p}_T/2$ . Using the approximation,  $\mathbf{k}_T \cdot \Delta \mathbf{p}_T = (\mathbf{p}_{1T}^2 - \mathbf{p}_{2T}^2)/2 \approx 0$ , we rewrite the terms on the transverse momenta in Eq.(32) as follows

$$\begin{aligned} & -U_{11}\mathbf{p}_{1T}^2 - U_{22}\mathbf{p}_{2T}^2 + 2U_{12}\mathbf{p}_{1T}\mathbf{p}_{2T} \\ & = -(U_{11} + U_{22} - 2U_{12})\mathbf{k}_T^2 - (U_{11} + U_{22} + 2U_{12})\Delta \mathbf{p}_T^2/4. \end{aligned}$$

After the integral for  $\mathbf{p}_{1T}$  in Eq.(31) is replaced by that for  $\mathbf{k}_T$ , the condition that  $|\mathbf{k}_T|$  ( $=k_T$ ) is approximately constant,  $|\mathbf{k}_T| \approx c$ , is introduced into Eq.(31);

$$\begin{aligned} G(\Delta y, \Delta \mathbf{p}_T) &= \int F(y_1, \mathbf{p}_{1T}, y_1 + \Delta y, \mathbf{p}_{1T} + \Delta \mathbf{p}_T) dy_1 \Big|_{|\mathbf{k}_T| \approx c} \\ &= \frac{C_0 \sqrt{\pi}}{\sqrt{A_{11} + A_{22} - 2A_{12}}} \exp \left[ -\frac{A_{11}A_{22} - A_{12}^2}{A_{11} + A_{22} - 2A_{12}} \Delta y^2 \right] \\ &\quad \times \exp \left[ -(U_{11} + U_{22} + 2U_{12})\Delta \mathbf{p}_T^2/4 - (U_{11} + U_{22} - 2U_{12})\mathbf{k}_T^2 \right]. \end{aligned} \quad (33)$$

The width of  $|\mathbf{k}_T|$  is neglected in Eq.(33), because it is canceled out in Eq.(31).

## VI. ANALYSIS OF EXPERIMENTAL DATA

The ALICE collaboration reported the observed charged multiplicity distribution [14] within the pseudo-rapidity range  $|\eta| < 1.0$  and the observed two-particle Bose-Einstein correlations [13] within  $|\eta| < 1.2$  in  $pp$  collisions at  $\sqrt{s} = 7$  TeV. We analyze the data on Bose-Einstein correlations within  $|\eta| < 1.2$ , using the parameters estimated from the observed MD within  $|\eta| < 1.0$ .

In order to analyze the observed MD by Eq.(23), we extract data of even prongs and renormalized those data to 1, because Eq.(23) is for identical particles. The result on the minimum chi-squared fit is  $\chi_{\min}^2/\text{nof} = 81.818/(35 - 4)$  at  $p_{\text{sm}} = 9.15$ ,  $\langle n_0 \rangle = 0.863$ ,  $h_L = 9.36 \times 10^{-5}$  and  $h_T = 9.34 \times 10^{-5}$ . Estimated values of  $\gamma_L$  and  $\gamma_T$  become so small that we cannot fit observed Bose-Einstein correlations for longitudinal and sideward directions.

Then, we use Eq.(28), the KNO-scaling function for the Glauber-Lachs formula, because we can use the published data without modification, and identify the scaling variable  $z_{\text{ch}} =$

TABLE I. Estimated parameters in the analysis of charged MD observed in  $pp$  collisions at  $\sqrt{s} = 7$  TeV [14].

$\langle n_{\text{ch}} \rangle$	$p_{\text{in}}$	$\chi^2_{\text{min}}/\text{nof}$
$12.11 \pm 0.09$	$0.654 \pm 0.021$	$235.3/(65-2)$

$n_{\text{ch}}/\langle n_{\text{ch}} \rangle$  for charged particles with  $z = n/\langle n \rangle$  for identical particles (for example negatively charged particles), where  $\langle n_{\text{ch}} \rangle = 2\langle n \rangle$ .

We analyze the MD observed in  $pp$  collisions at  $\sqrt{s} = 7$  TeV by  $P(n) = \phi(z)/\langle n_{\text{ch}} \rangle$ , where  $\phi(z)$  is given by Eq.(30). The estimated parameters in the analysis are shown in Table I. The observed MD is compared with  $P(n)$  calculated by Eq.(30) in Fig.1.

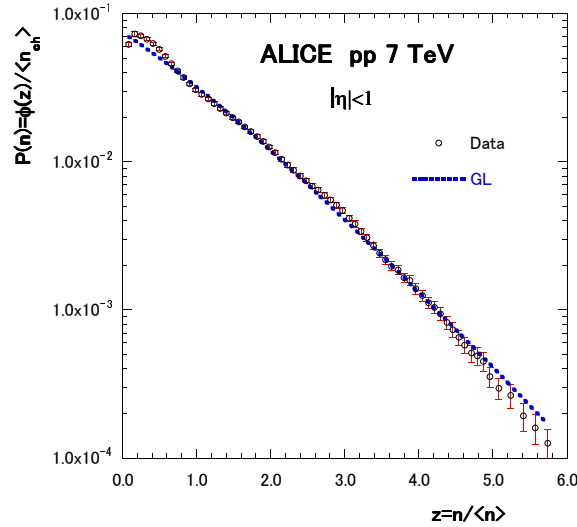


FIG. 1. Analysis of charged MD in  $pp$  collisions at  $\sqrt{s} = 7$  TeV by Eq.(30).

As can be seen from Eqs.(24) and (27), the estimated values of  $\langle n_{\text{ch}} \rangle$  (or  $\langle n \rangle = \langle n_{\text{ch}} \rangle/2$ ) and  $p_{\text{in}}$  gives two constraints on the parameters,  $p_{\text{sm}}$ ,  $\langle n_0 \rangle$ ,  $h_L$  and  $h_T$ . When we analyze the observed data on two-particle Bose-Einstein correlations with 4 parameters,  $\alpha$ ,  $\beta$ ,  $h_L$  and  $h_T$ , values of  $h_L = \gamma_L/\alpha$  and  $h_T = \gamma_T/\beta$  sometimes show unstable behaviors. Therefore we fix at  $\alpha = 0.25$  and  $\beta = 50$ . Then, we analyze the data with two parameters,  $h_L$  and  $h_T$ .

The parameters  $p_{\text{sm}}$  and  $\langle n_0 \rangle$  are given by the following equations,

$$p_{\text{sm}} = \frac{\xi f_2}{A_0 f_1 + \xi f_2}, \quad \langle n_0 \rangle = \frac{A_0 f_1 + \xi f_2}{f_1 f_2}.$$

In the above equations,  $\xi$  and  $A_0$  depend only on  $p_{\text{in}}$  and  $\langle n \rangle$ , whereas  $f_1$  and  $f_2$  depend

only on  $\gamma_L/\alpha$  and  $\gamma_T/\beta$ ;

$$\begin{aligned}\xi &= p_{\text{in}}\langle n \rangle / (1 + p_{\text{in}}\langle n \rangle), \quad A_0 = (1 - p_{\text{in}})\langle n \rangle / (1 + p_{\text{in}}\langle n \rangle)^2, \\ f_1 &= (1 - \sqrt{r_1/r_2})(1 - \sqrt{t_1/t_2})^2, \quad f_2 = \sqrt{1 - r_1/r_2}(1 - t_1/t_2).\end{aligned}$$

The two-particle Bose-Einstein correlations in  $pp$  collisions are measured in longitudinal, sideward and outward directions. In  $pp$  collisions, data would be almost the same in  $q_{\text{side}}$  and  $q_{\text{out}}$  directions. Therefore, the data in  $q_{\text{long}}$  and  $q_{\text{side}}$  directions are analyzed. We compare the calculated results for  $n = 4, 10$  and  $17$  with the data for  $n_{\text{ch}}$  from 1 to 11, from 17 to 22 and from 29 to 34, respectively.

In the analysis of two-particle Bose-Einstein correlations, we use the identity  $\Delta \mathbf{p}_T^2 = q_{\text{side}}^2 + q_{\text{out}}^2$  and the following approximate relations,

$$\begin{aligned}q_{\text{long}}^2 &= 2\langle m_T^2 \rangle (\cosh \Delta y - 1), \\ \Delta y &= \ln(a \pm \sqrt{a^2 - 1}), \quad a = \frac{q_{\text{long}}^2}{2\langle m_T^2 \rangle} + 1,\end{aligned}\tag{34}$$

where  $\langle m_T^2 \rangle = 0.14^2 + 0.2^2 = 0.0596 \text{ (GeV/c)}^2$ .

Data on  $C_n^{(2)}(q_{\text{long}})$  are taken with the  $k_T$  range  $(k_{T1}, k_{T2}) \text{ GeV/c}$ ,  $|q_{\text{side}}| < 0.16 \text{ GeV/c}$  and  $|q_{\text{out}}| < 0.16 \text{ GeV/c}$ . In order to take these conditions into account, we use  $\mathbf{k}_T^2 = (k_{T1}^2 + k_{T2}^2)/2$ ,  $\Delta \mathbf{p}_T^2 = q_{\text{side}}^2 + q_{\text{out}}^2 = 0^2 + 0.16^2 = 0.0256 \text{ (GeV/c)}^2$  in Eq.(33). Data on  $C_n^{(2)}(q_{\text{side}})$  are taken with the  $k_T$  range,  $(k_{T1}, k_{T2}) \text{ GeV/c}$ ,  $|q_{\text{long}}| < 0.16 \text{ GeV/c}$  and  $|q_{\text{out}}| < 0.16 \text{ GeV/c}$ . In this case, we use  $\mathbf{k}_T^2 = (k_{T1}^2 + k_{T2}^2)/2$  and  $q_{\text{long}}^2 = q_{\text{out}}^2 = 0.0128 \text{ (GeV/c)}^2$  in Eqs.(33) and (34).

The results on  $C_n^{(2)}(q_{\text{long}})$  are shown in Table II and Fig.2. As the data are taken with  $k_T$  range  $(0.2, 0.3) \text{ GeV/c}$ ,  $|q_{\text{side}}| < 0.16 \text{ GeV/c}$  and  $|q_{\text{out}}| < 0.16 \text{ GeV/c}$ , we put  $\mathbf{k}_T^2 = 0.065 \text{ (GeV/c)}^2$  and  $\Delta \mathbf{p}_T^2 = 0.0256 \text{ (GeV/c)}^2$  in Eq.(33). In the minimum chi-squared fit, data points with  $q_{\text{long}} < 0.6 \text{ GeV/c}$  (15 points) are used. All the values of parameters,  $p_{\text{sm}}$ ,  $\langle n_0 \rangle$ ,  $h_L$  and  $h_T$  estimated in the analysis of  $C_n^{(2)}(q_{\text{long}})$  increase as multiplicity  $n$  increases. It should be noted that the MD defined by Eq.(23) is contained in the formula of the two-particle BEC function given by Eq.(31), and it calculated from Eq.(23) with parameters shown in Table II becomes broader as multiplicity  $n$  increases.

The results on  $C_n^{(2)}(q_{\text{side}})$  are shown in Table III and Fig.3. As the data are taken with  $k_T$  range  $(0.2, 0.3) \text{ GeV/c}$ ,  $|q_{\text{long}}| < 0.16 \text{ GeV/c}$  and  $|q_{\text{side}}| < 0.16 \text{ GeV/c}$ , we put  $\mathbf{k}_T^2 = 0.065$  and  $\Delta \mathbf{p}_T^2 = 0.0256$  in Eq.(33). In the minimum chi-squared fit, data points with  $q_{\text{long}} < 1$

TABLE II. Estimated parameters in  $C_n^{(2)}(q_{\text{long}})$  observed in  $pp$  collisions [13] at  $\sqrt{s} = 7$  TeV.

parameters	$n = 4$	$n = 10$	$n = 17$
$p_{\text{sm}}$	$0.969 \pm 0.004$	$0.975 \pm 0.003$	$0.978 \pm 0.003$
$\langle n_0 \rangle$	$3.78 \pm 0.10$	$4.93 \pm 0.12$	$6.07 \pm 0.12$
$h_L$	$5.13 \pm 0.29$	$6.56 \pm 0.34$	$8.29 \pm 0.38$
$h_T$	$0.351 \pm 0.014$	$0.543 \pm 0.013$	$0.698 \pm 0.001$
$\chi^2_{\text{min}}/\text{nof}$	$99.1/(15 - 2)$	$84.0/(15 - 2)$	$34.8/(15 - 2)$

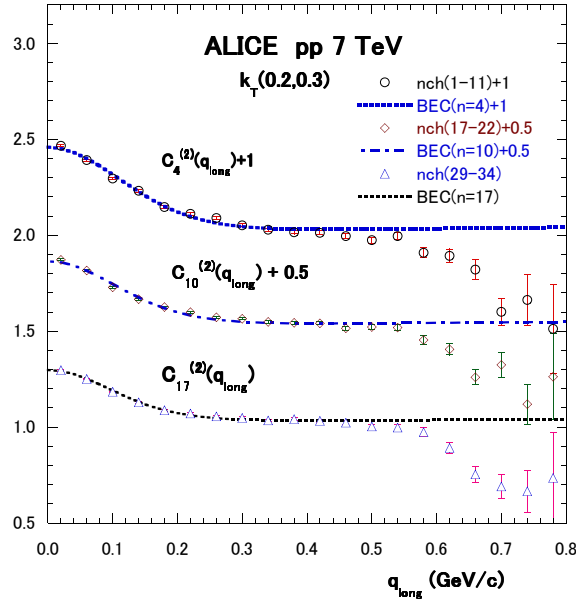


FIG. 2. Analysis of  $C_n^{(2)}(q_{\text{long}})$  in  $pp$  collisions at  $\sqrt{s} = 7$  TeV by Eq.(31).

GeV/c (25 points) are used. All the values of parameters estimated in the analysis increase, as multiplicity  $n$  increases. The MD calculated from Eq.(23) with parameters shown in Table III also becomes broader as multiplicity  $n$  increases.

The results on the  $k_T$  dependence of  $C_{10}^{(2)}(q_{\text{long}})$  are shown in Table IV and Fig.4. All the values of parameters increase as  $k_T$  increases. In this case, the MD calculated from Eq.(23) with parameters shown in Table IV becomes narrower as  $k_T$  increases.

The results on  $k_T$ -dependence of the Bose-Einstein correlations in the sideward direction are shown in Table V and in Fig.5. All the values of parameters decrease as  $k_T$  increases. The MD calculated from Eq.(23) with parameters shown in Table IV becomes narrower as

TABLE III. Estimated parameters in  $C_n^{(2)}(q_{\text{side}})$  observed in  $pp$  collisions at  $\sqrt{s} = 7$  TeV [13].

parameters	$n = 4$	$n = 10$	$n = 17$
$p_{\text{sm}}$	$0.963 \pm 0.004$	$0.971 \pm 0.003$	$0.976 \pm 0.003$
$\langle n_0 \rangle$	$3.14 \pm 0.05$	$4.53 \pm 0.10$	$5.79 \pm 0.1$
$h_L$	$6.76 \pm 0.19$	$10.8 \pm 0.3$	$14.4 \pm 0.5$
$h_T$	$0.106 \pm 0.007$	$0.241 \pm 0.016$	$0.357 \pm 0.022$
$\chi^2_{\text{min}}/\text{nof}$	$142.1/(25 - 2)$	$84.0/(25 - 2)$	$34.8/(25 - 2)$

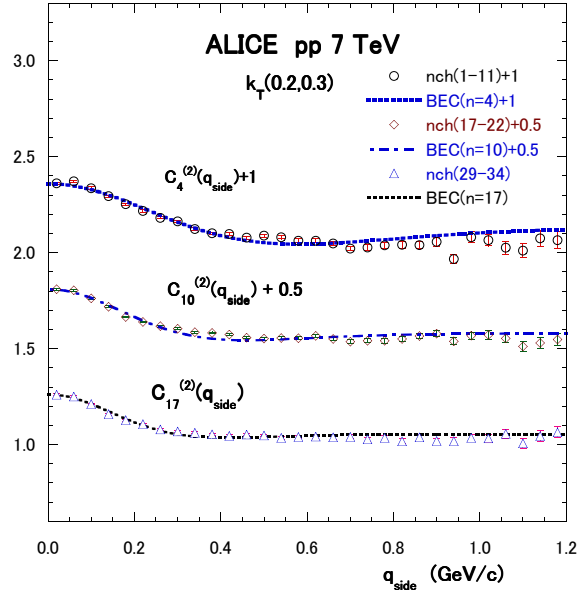


FIG. 3. Analysis of  $C_n^{(2)}(q_{\text{side}})$  in  $pp$  collisions at  $\sqrt{s} = 7$  TeV by Eq.(31).

$k_T$  increases.

The source radii,  $R_l$  for the longitudinal direction and  $R_s$  for the sideward direction are defined by the following equations,

$$R_l = \sqrt{\gamma_L / \langle m_T^2 \rangle}, \quad R_s = \sqrt{\gamma_T}.$$

The multiplicity  $n$  dependences of source radii calculated from  $\gamma_L$  and  $\gamma_T$ , which are estimated in the analysis of  $C_n^{(2)}(q_{\text{long}})$ , are shown in Fig.6. Source radii  $R_l$  and  $R_s$  increase as multiplicity  $n$  increases. Values of  $R_l$  and  $R_s$  at each  $n$  coincide within the error bars.

The  $n$  dependences of source radii calculated from  $\gamma_L$  and  $\gamma_T$  in the analysis of  $C_n^{(2)}(q_{\text{side}})$  are shown in Fig.7. Both radii increase with multiplicity  $n$ . At each  $n$ ,  $R_l$  is greater than

TABLE IV. Estimated parameters in  $C_{10}^{(2)}(q_{\text{long}})$  observed in  $pp$  collisions at  $\sqrt{s} = 7$  TeV [14].

$C_{10}^{(2)}(q_{\text{long}})$	$k_T = (02, 03)\text{GeV}$	$k_T = (04, 05)\text{GeV}$	$k_T = (06, 07)\text{GeV}$
$p_{\text{sm}}$	$0.974 \pm 0.003$	$0.967 \pm 0.004$	$0.955 \pm 0.005$
$\langle n_0 \rangle$	$4.70 \pm 0.12$	$3.34 \pm 0.09$	$2.21 \pm 0.03$
$h_L$	$5.88 \pm 0.35$	$3.66 \pm 0.24$	$1.87 \pm 0.14$
$h_T$	$0.537 \pm 0.014$	$0.355 \pm 0.012$	$0.189 \pm 0.012$
$\chi_{\text{min}}^2/\text{nof}$	$110.7/(15 - 2)$	$91.0/(25 - 2)$	$47.1/(25 - 2)$

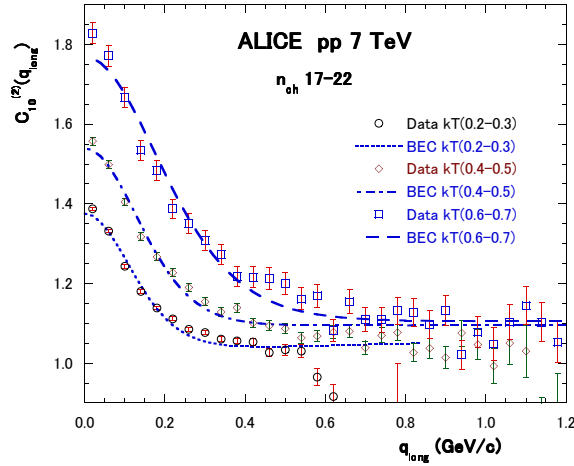


FIG. 4. Analysis of  $C_{10}^{(2)}(q_{\text{side}})$  in  $pp$  collisions at  $\sqrt{s} = 7$  TeV by Eq.(31).

TABLE V. Estimated parameters in  $C_{10}^{(2)}(q_{\text{side}})$  observed in  $pp$  collisions at  $\sqrt{s} = 7$  TeV [14].

$C_{10}^{(2)}(q_{\text{side}})$	$k_T = (02, 03)\text{GeV}$	$k_T = (04, 05)\text{GeV}$	$k_T = (06, 07)\text{GeV}$
$p_{\text{sm}}$	$0.971 \pm 0.003$	$0.967 \pm 0.004$	$0.959 \pm 0.005$
$\langle n_0 \rangle$	$4.35 \pm 0.11$	$3.66 \pm 0.11$	$2.67 \pm 0.12$
$h_L$	$10.3 \pm 0.34$	$8.45 \pm 0.47$	$4.75 \pm 0.52$
$h_T$	$0.223 \pm 0.018$	$0.151 \pm 0.014$	$0.0894 \pm 0.0089$
$\chi_{\text{min}}^2/\text{nof}$	$259.8/(25 - 2)$	$148.4/(25 - 2)$	$98.1/(25 - 2)$

$R_s$ .

The  $k_T$  dependences of source radii  $R_l$  and  $R_s$  calculated from  $\gamma_L$  and  $\gamma_T$  in the analysis of  $C_{10}^{(2)}(q_{\text{long}})$  are shown in Fig.8. Both radii decrease as  $k_T$  increases. The source radius  $R_l$

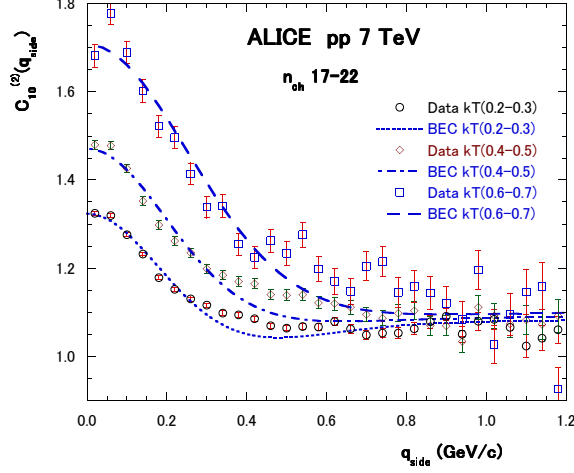


FIG. 5. Analysis of  $C_n^{(2)}(q_{side})$  in  $pp$  collisions at  $\sqrt{s} = 7$  TeV by Eq.(31).

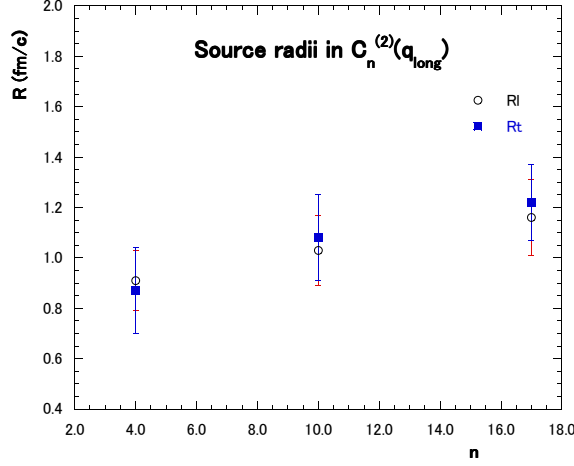


FIG. 6. Source radii  $R_l$  and  $R_s$  in the analysis of  $C_n^{(2)}(q_{long})$ , which are calculated from  $\gamma_L$  and  $\gamma_T$  shown in Table II.

is equal to  $R_s$  within the error bars at each  $k_T$ .

The  $k_T$  dependences of source radii  $R_l$  and  $R_s$  calculated from  $\gamma_L$  and  $\gamma_T$  in the analysis of  $C_{10}^{(2)}(q_{side})$  are shown in Fig.9. Both radii decrease as  $k_T$  increases.  $R_l$  is greater than  $R_s$  at each  $k_T$ .

## VII. SUMMARY AND DISCUSSIONS

The charged multiplicity distribution in  $|\eta| < 1$  and the two-particle Bose-Einstein correlations at fixed multiplicities in  $|\eta| < 1.2$  observed in  $pp$  collisions at  $\sqrt{s} = 7$  TeV by the

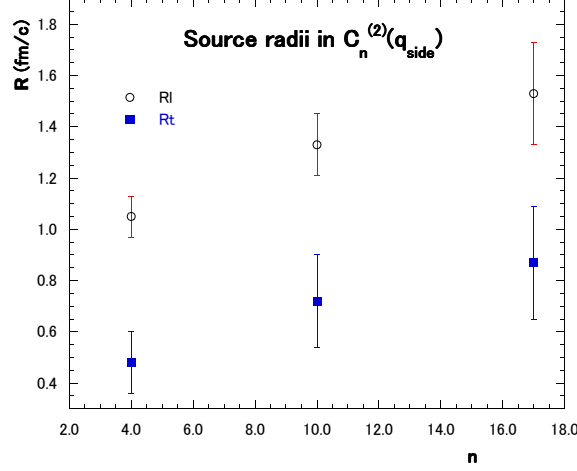


FIG. 7. Source radii  $R_l$  and  $R_s$  in the analysis of  $C_n^{(2)}(q_{side})$ , which are calculated from  $\gamma_L$  and  $\gamma_T$  shown in Table III.

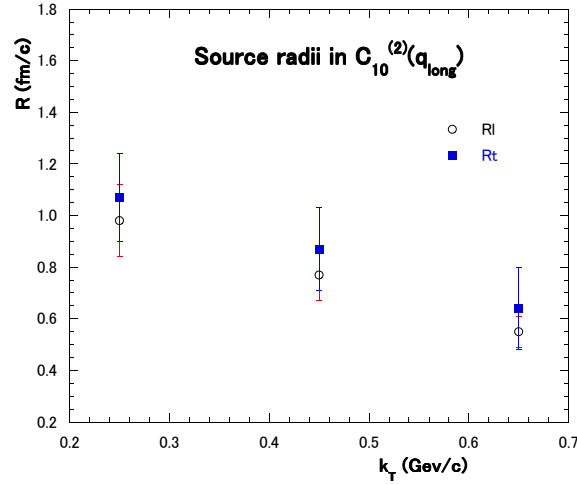


FIG. 8. Source radii  $R_l$  and  $R_s$  in the analysis of  $C_{10}^{(2)}(q_{long})$ . The radii are calculated from  $\gamma_L$  and  $\gamma_T$  shown in Table IV.

ALICE Collaboration are analyzed by the formulae obtained in the QO approach. At first, the observed charged MD is analyzed by the KNO scaling function of the Glauber-Lach formula. It is approximately derived from the recurrence equation for the MD, and contains two parameters, the chaoticity parameter  $p_{in}$  in the inclusive events and the average multiplicity  $\langle n \rangle$  of negatively charged particles. Those two parameters give two constraints on the chaoticity parameter  $p_{sm}$  in the semi-inclusive events, the normalization factor  $\langle n_0 \rangle$ ,  $h_L = \gamma_L/\alpha$  and  $h_T = \gamma_T/\beta$ . Parameters  $\alpha$  and  $\beta$  are related to the width of rapidity and  $p_T$  distributions, respectively. Those are fixed at  $\alpha = 0.25$  and  $\beta = 50$ . The parameter  $\gamma_L$



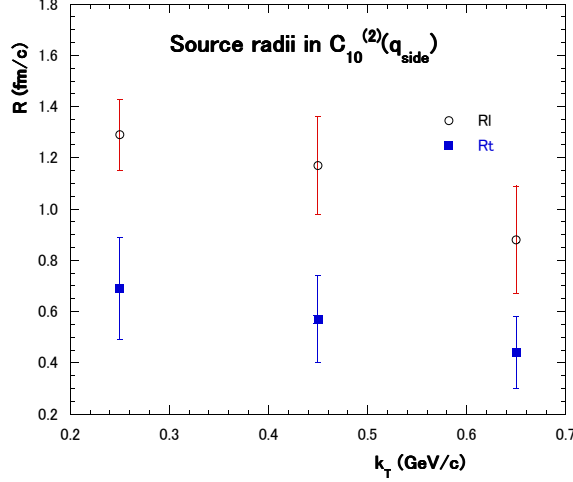


FIG. 9. Source radii  $R_l$  and  $R_s$  in the analysis of  $C_{10}^{(2)}(q_{side})$ . The radii are calculated from  $\gamma_L$  and  $\gamma_T$  shown in Table V.

is related to the longitudinal source radius and  $\gamma_T$  is related to the transverse radius. Using parameters  $h_L$  (or  $\gamma_L$ ) and  $h_T$  (or  $\gamma_T$ ), we can analyze the data on two-particle Bose-Einstein correlations for the longitudinal direction and the sideward (or outward) direction. As the data are taken in  $pp$  collisions, we neglect the difference between the correlations in the sideward direction and those in the outward direction.

In our formulation of the BEC function, restrictions on  $k_T$ ,  $q_{out}$ ,  $q_{side}$  and so forth are taken into account. Therefore, even in the analysis of two-particle Bose-Einstein correlations in the longitudinal direction, we can estimate the source radius  $R_s$  in addition to the source radius  $R_l$ .

From the analysis of the Bose-Einstein correlations in the longitudinal direction, estimated values of  $R_l$  and  $R_s$  coincide with each other at each multiplicity  $n$  or  $k_T$ . On the other hand, from the analysis of the Bose-Einstein correlations in the sideward direction, estimated values of  $R_l$  are greater than those of  $R_s$  at each multiplicity  $n$  or  $k_T$ . Both radii increase as multiplicity  $n$  increases. On the other hand, both radii decrease as  $k_T$  increases.

In the analysis of observed two-particle Bose-Einstein correlations at fixed multiplicities, the MD calculated from Eq.(23) becomes broader as multiplicity  $n$  increases, whereas it becomes narrower as  $k_T$  increases. The behavior of calculated multiplicity distributions suggests that the data selection conditions in the observed two-particle Bose-Einstein correlations would have non-negligible effects on the shape of observed multiplicity distributions.

If the MD, one-particle and two-particle momentum densities are constructed from the same data samples, or at least from the data in the same pseudo-rapidity range, values of parameters would be estimated more consistently.

## ACKNOWLEDGMENTS

One of the authors (N.S.) would like to thank A. Kiesel for his kind correspondence. He also thanks S. Muroya for his valuable comments.

- 
- [1] S. Pratt, Phys. Lett. **B301**, 159(1993).
  - [2] Q. H. Zhang, Phys. Lett., B406, 366(1997).
  - [3] T. Csörgő and J. Zimanyi, Phys. Rev. Lett. **80**, 916(1998), J. Zimanyi and T. Csörgő, Heavy Ion Physics, **9**, 241(1999).
  - [4] R. Lednicky et al., Phys. Rev. **C61**, 034901(2000).
  - [5] R. J. Glauber, Phys. Rev. **131**, 2766(1963); Optical Coherence and Photon Statistics, in Quantum Optics and Electronics, Les Houches, 1964 edited by C. De Witt, et al. (New York, 1965), p.63; G. Lachs, Phys. Rev., **138**, B1012(1965).
  - [6] M. Biyajima, O. Miyamura and T. Nakai, Proceedings of the Multiparticle Dynamics, Hakone, Japan, 1978 (PIFP, Kyoto Univ., Japan, 1978), p.139.
  - [7] M. Biyajima, A. Bartl, T. Mizoguchi, N. Suzuki and O. Terazawa, Prog. Theor. Phys. **84**, 931(1990); *ibid.* **88**, 157(1992).
  - [8] N. Suzuki, M. Biyajima and I. V. Andreev, Phys. Rev. **C56**, 2736(1997); N. Suzuki and M. Biyajima, Prog. Theor. Phys. **88**, 609(1992).
  - [9] N. Suzuki and M. Biyajima, Phys. Rev. **C60**, 034903(1999); Proceedings of the 8-th International Symposium on Multiparticle Production "Correlations and Fluctuations '98" at Matrahaza, Hungary, 1998, Eds. T. Csörgő, S. Hegyi, R. Hwa and G. Jancsó, World Scientific, pp.98-107.
  - [10] N. Suzuki, M. Biyajima and T. Mizoguchi, Phys. Part. Nucl. Lett. **8**, 1007(2011).
  - [11] M. Namiki, I. Ohba and N. Suzuki, Prog. Theor. Phys. **53**, 775(1975); M. Biyajima and N. Suzuki, Prog. Theor. Phys. **73**, 918(1985).

- [12] Z. Koba, H. B. Nielsen and P. Olesen, Nucl. Phys. **B43**, 125(1972); Z. Koba, Acta Phys. Pol. B4, 95(1973). L. S. Brown, Phys. Rev. **D5**, 748(1972).
- [13] ALICE Collaboration, K. Aamodt, et al., Phys. Rev. D**84**, 112004(2011).
- [14] ALICE Collaboration, K. Aamodt, et al., Eur. Phys. J. C**68**, 345(2010).